Enhancing the hardness of Al/W nanostructured coatings

2009 J. Phys.: Condens. Matter 21 055003

(http://iopscience.iop.org/0953-8984/21/5/055003)

J. Phys.: Condens. Matter **21** (2009) 055003 (9pp) doi:10.1088/0953-8984/21/5/055003

Enhancing the hardness of Al/W nanostructured coatings

F A Burgmann[1], D G McCulloch[1], L Ryves[2], S H N Lim[2], D R McKenzie[2] and M M M Bilek[2]

[1] Applied Physics, School of Applied Sciences, RMIT University, City Campus, GPO Box 2476V, Melbourne, 3001 VIC, Australia
[2] Applied and Plasma Physics, School of Physics (A28), University of Sydney, Sydney, 2006 NSW, Australia

Received 28 July 2008, in final form 31 October 2008
Published 16 December 2008
Online at stacks.iop.org/JPhysCM/21/055003

Abstract
Two-component multilayer thin films frequently show hardness enhancements at specific repeat periods above that of the constituent layers. This study of hardness enhancements in W/Al nanostructured coatings provides strong new evidence that hardness enhancements in this system arise not only from the presence of a layered structure, but also from the presence of defects introduced by changing the deposition conditions. Samples with well defined layers of W and Al were produced by sputtering to cover a wide range of periods from 10 to 200 nm. No evidence of enhanced hardness in these films was found by nanoindentation. On the other hand, samples deposited from cathodic arc sources showed strong hardness enhancement above that of pure W. However, the samples of highest hardness did not contain Al layers for much of their thickness. The hardening mechanism therefore could not be attributed to the presence of a multilayer structure. Examination of the microstructure showed that the interruptions to the W deposition caused by operation of the Al source introduced defects which acted as pinning sites for dislocations. The nanoindentation hardness data were well described using a modified Hall–Petch relation.

1. Introduction

Thin film multilayer structures with layer thicknesses on the nanometre scale have, under some conditions, exhibited increased hardness and fracture toughness compared to either of the constituent layers [1–4]. Of particular interest are multilayers of materials such as metals and their nitrides which are reported to show a hardness enhancement when the multilayer repeat distance (period, λ) is of the order of 2–5 nm [5–8]. The mechanisms that lead to this hardness enhancement are not yet well understood. In order to understand these mechanisms, a first step is to identify relationships between microstructure and mechanical properties. The importance of studying microstructure is underscored by recent observations [9] in which it was found that the formation of a multilayer structure is not guaranteed where two different materials are deposited alternately. For example, the expected multilayer structure was not obtained in Al/AlN for periods below 15 nm, instead the Al formed islands in a matrix of AlN [9].

The AlO_x/W multilayer system (where x is the fraction of O) is of interest from several viewpoints [10]. If $x = 0$, both layers are metallic and have contrasting mechanical properties. Al is ductile with a low yield strength while W is one of the hardest metals. When $x > 0$, the layers have very different crystallography so that crack propagation should be arrested at the interfaces. In this paper, we explore the formation of AlO_x/W multilayer coatings as a function of the layer periods, prepared using two different physical vapour deposition methods: pulsed magnetron sputtering and pulsed filtered cathodic arc. The differences between these two techniques are significant. Cathodic arc deposited films are formed from energetic ions with energies in the range of 20–120 eV [11, 12], while sputtered films are deposited primarily from low energy neutrals [13]. The incident energy of the depositing particles is known to have an important influence on the stress generated within the films and on the microstructure [14, 15].

2. Experimental details

Two techniques, sputtering and cathodic arc deposition were used to produce multilayer coatings with a nominal total film

thickness of 200 nm. A set of multilayer samples was prepared by varying λ from 10 to 200 nm using pulsed magnetron sputtering [13]. These samples are referred to as S10 to S200. Two sputter guns with 76 mm diameter Al and W targets were run alternately in pulsed-DC mode using an Advanced Energy Pinnacle Plus power supply operating at a frequency of 100 kHz with an average power of 100 W. The substrate was mounted on a holder which was moved to alternately bring the substrate in line with the target that was powered. To achieve comparable deposition rates for both the Al and W, the Ar flow rates and the resultant chamber pressures were adjusted to 126 sccm and 6.9 mTorr, and 89 sccm and 4.5 mTorr, respectively. Prior to deposition, the ⟨100⟩ Si substrates were ultrasonically cleaned in acetone and dried in pure nitrogen. The chamber was cryogenically pumped: the residual pressure was 7×10^{-6} Torr.

A set of samples (labelled with the prefix 'A') was prepared using a pulsed filtered cathodic arc deposition system [16] operating in the absence of intentionally introduced gases. Samples A1 to A200 were prepared with varying λ from 1 to 200 nm. This system has two cathodes injecting plasma into the same filter duct, so that multilayered materials can be deposited without breaking vacuum between layers. The Al and W cathodes were triggered with a repetition rate of 5 pulses per second by applying a high voltage trigger pulse to an electrode mounted at the centre of each cathode. The cathodic arc was driven by a high current (1.5 kA) power supply. Since the two materials have different arc spot velocities, two different pulse lengths of 250 and 500 μs were used for Al and W, respectively. This produced average deposition rates of 0.024 nm per arc pulse for Al and 0.008 nm per arc pulse for W. The multilayers were deposited on either ⟨100⟩ Si wafers or ⟨100⟩ Si wafers with a 500 nm SiO_2 surface layer. All substrates were chemically cleaned using acetone, ethanol and distilled water baths in an ultrasonic cleaner. The substrate was allowed to reach floating potential during deposition. Prior to deposition, the residual chamber pressure was approximately 3×10^{-6} Torr.

Two additional sets of samples (labelled with the prefixes 'Ar' and 'O') were prepared in the pulsed filtered cathodic arc deposition system in the presence of Ar and O_2 gas respectively. In the case of the 'Ar' samples, Ar gas was admitted into the chamber after the deposition of each W layer at a flow rate which produced a chamber pressure of approximately 1×10^{-3} Torr. The Al cathode was then pulsed 500 times to initiate Al deposition onto the W surface. The deposition was monitored using *in situ* ellipsometry. Once initial deposition was observed, the Ar flow was turned off for the remainder of the Al layer deposition. In the case of the 'O' samples, O_2 gas was admitted to the chamber after the deposition of each W layer to bring the chamber to atmospheric pressure over a period of 5 min. The chamber was then pumped down again to a base pressure of 10^{-6} Torr before the deposition of the Al layer was commenced.

The composition of the films was determined using Auger electron spectroscopy (AES) depth profiling. A scanning Auger Nanoprobe VG 310F fitted with ion sputtering capabilities was used to obtain depth profiles using a 3 keV Ar ion beam. The microstructure of the coatings was investigated using cross-sectional transmission electron microscopy (XTEM). Cross-sectional specimens were prepared either using the 'lift-out' technique in a focused ion beam (FIB) system [17] or by mechanical polishing and Ar ion beam thinning. The samples were then examined in cross-section using transmission electron microscopy (TEM) and scanning TEM (STEM) in combination with electron energy loss spectroscopy (EELS) and energy dispersive spectroscopy (EDS). X-ray diffraction was performed using a Bruker AXS D8 ADVANCE wide angle x-ray diffractometer using Cu kα x-rays.

A Hysitron TriboIndenter with a diamond Berkovich indentation tip was used to determine the hardness and elastic modulus. Twenty five indentations were performed, creating a 5 × 5 matrix of indentations, each 15 μm^2 in area. Forces ranging between 2000 and 150 μN were applied at a scan rate of 1–2 Hz. To minimize the effect of the substrate and to normalize for different total film thicknesses, the values resulting from indentation with penetration depths of 15% of the film thickness or less were used.

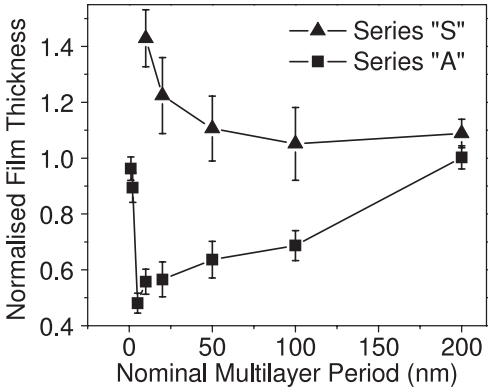

Figure 1. Normalized deposited film thickness, defined as the actual deposited film thickness divided by the anticipated film thickness (based on the individual deposition rates of Al and W), plotted against nominal film period for sputtered ('S' series) and arc ('A' series) Al/W multilayers. The 'nominal film period' is the period calculated from the anticipated film thickness of an Al and W bilayer. The error bars represent three standard deviations obtained from several thickness measurements using a profilometer.

3. Results

Figure 1 shows the actual deposited film thickness divided by the anticipated film thickness (based on the individual deposition rates of Al and W), plotted against nominal film period for the sputtered (series 'S') and the arc (series 'A') sample sets. The 'nominal film period' is the period calculated from the anticipated film thickness of an Al and W bilayer. For periods down to 50 nm, the actual deposited film thickness of the 'S' series showed good agreement with the anticipated film thickness. In the case of the samples with the smallest periods of 20 and 10 nm, the actual deposited film thickness was greater than the anticipated film thickness. This is likely to be the result of the time taken to shut off the deposition which

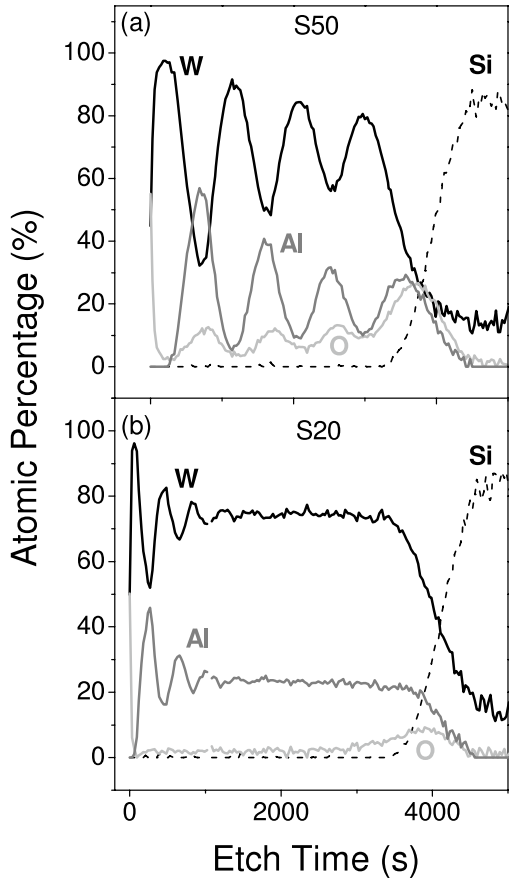

Figure 2. The atomic percentages of Al, O, Si and W determined using AES depth profiling for the sputtered ('S' series) samples, (a) sample S50 and (b) sample S20.

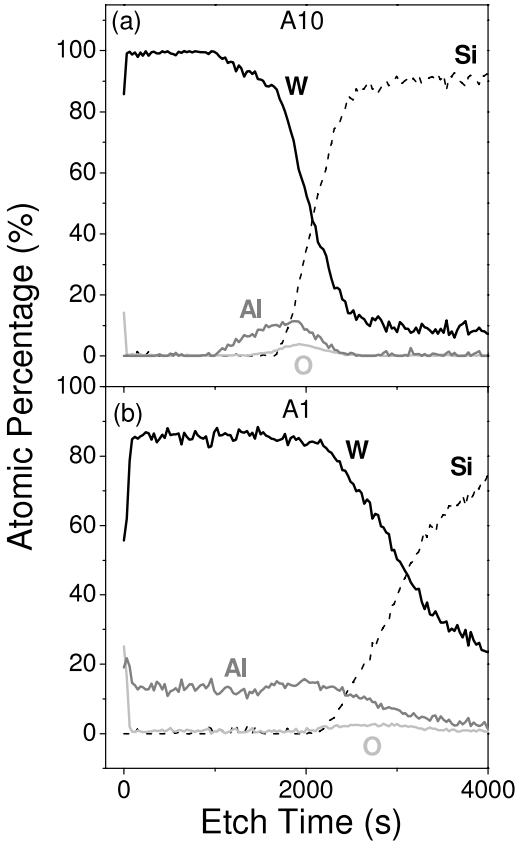

Figure 3. The atomic percentages of Al, O, Si and W determined using AES depth profiling for the arc ('A' series) samples, (a) sample A10 and (b) sample A1.

becomes significant at small layer thicknesses. The 'A' samples have measured coating thicknesses which were less than the nominal values, down to approximately 50% in the case of the sample with a nominal period of 5 nm. The measured thickness of the samples with a nominal period of 2 and 1 nm increased rapidly, approaching the nominal thickness. As shown below, the deficit in deposited thicknesses is due to the absence of most of the Al layers.

Compositional analysis performed using AES depth profiling of the S50 and S20 sputtered samples is shown in figure 2. The profile of the S50 sample clearly shows that a layered structure is present. The profile of the S20 sample shows initial oscillations resulting from layers which disappear with increasing depth. This could be the result of the combined effects of roughening of the etch crater as the sputtering time increases and of layer roughness. The AES results for both films show incorporation of O, particularly into the Al layers which oxidize readily.

Figure 3(a) shows the AES profile for the sample A10. No Al is present near the surface of the sample. The only Al seen within this sample is near the Si substrate, indicating that Al is only incorporated during the initial stages of deposition, in agreement with the observation of a deficiency in total film thickness shown in figure 1. A similar deficiency of Al was observed for all 'A' series samples deposited with nominal periods of 5 nm or more. In the case of samples with nominal periods of 2 and 1 nm, Al was present throughout the entire coating as shown for the 1 nm case in figure 3(b).

Figures 4(a) and (b) show AES profiles for samples Ar25 and O20. In contrast to the 'A' series deposited in vacuum, the AES results show that the presence of either Ar or O_2 encourages the formation of multilayers. In the case of sample O20, there are high levels of O incorporated into the Al layers.

XTEM images of typical 'S' series samples are shown in figures 5(a)–(c). All samples show a distinct alternating layered structure of AlO_x/W throughout their thickness. The roughness of the interfaces gradually increases as the deposition progresses. XTEM images of samples A50, A10 and A1 are shown in figures 6(a)–(c). The sample A50 shows an initial Al layer of 25 nm, confirmed by energy loss near edge structure (ELNES) of the Al L edge, followed by a W layer of approximately 100 nm. This observation supports the AES results which show that Al is only present in the initial stages of deposition of 'A' series samples with $\lambda > 2$ nm. Figure 6(b) shows sample A10 which has thin Al layers near the Si substrate that decrease in thickness as the deposition proceeds. Figure 6(c) shows the sample A1, in which no layering can be discerned.

Figure 7 shows (a) a high angle annular dark field STEM image of sample A10 along with (b) an EDS line scan through several layers as indicated in (a). The EDS results show that

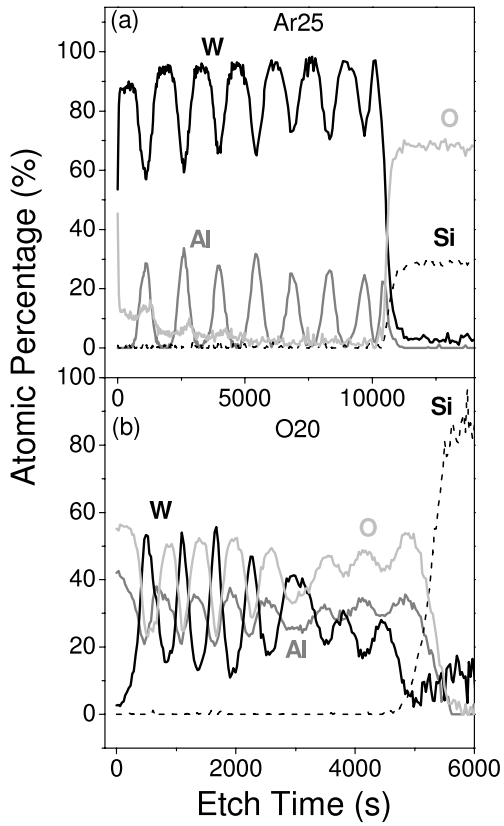

Figure 4. (a) The atomic percentages of Al, O, Si and W determined using AES depth profiling for the cathodic arc deposited samples prepared with Ar ('Ar' series) with a period of 25 nm (sample Ar25), and (b) the corresponding percentages for the arc deposited sample prepared with O_2 ('O' series) with a period of 20 nm (sample O20).

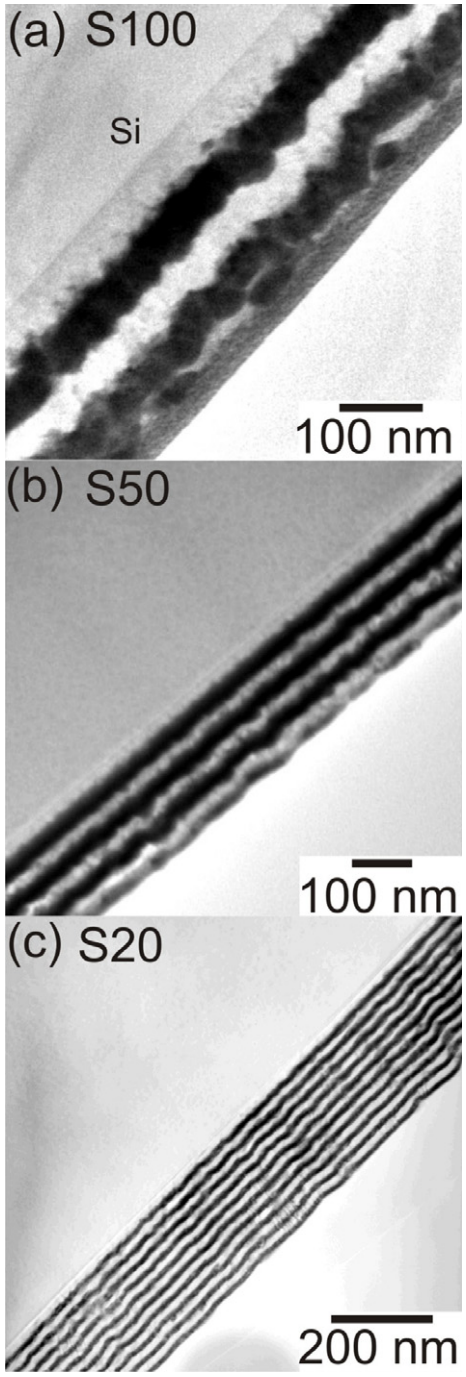

Figure 5. XTEM images of the 'S' series samples (a) S100, (b) S50 and (c) S20. Note that the Pt layer deposited during FIB XTEM specimen preparation is missing in (b) and (c), and the top most W layer has also been partially removed in (b).

O is present in the Al layers in decreasing concentration as deposition proceeds.

Figure 8 shows the x-ray diffraction pattern from sample A1. The x-ray diffraction pattern indicates that some W–Al intermetallic alloys have formed, with many lines indexable to Al_4W and Al_5W, in addition to pure W lines [18].

Figure 9 shows XTEM images of samples (a) Ar25 and (b) O20 together with (c) an EDS line scan across the initial layers of O20 as indicated in (b). Clearly the presence of either Ar or O_2 at the changeover from W to Al deposition increases the likelihood that an Al or AlO_x layer will form. The EDS line scan shows that in the O20 sample, during Al deposition, sufficient O_2 is incorporated to form an oxide that is close in stoichiometry to Al_2O_3.

Indentation hardness and elastic modulus are shown in figure 10 for all samples. The 'S' samples show no systematic dependence of indentation hardness and modulus on multilayer period. The hardness values of the 'S' series samples lie between those found for films of Al and W, and their modulus values are similar to that of pure Al. The 'A' samples show a contrasting behaviour. A peak occurs in both indentation hardness and modulus at a nominal multilayer thickness of 10 nm. The hardness value of the sample A10 is the highest at approximately 25 GPa, substantially higher than either of the two constituent materials. The elastic modulus values reached a peak of approximately 270 GPa for the sample with a period of 5 nm, again showing values higher than either Al or W. The hardness for the samples of finest nominal period is lower than the maximum, consistent with the formation of soft intermetallics as observed in figure 8 [18]. Also plotted in figures 10(a) and (b) are the modulus and hardness of the 'Ar' and 'O' samples. There is no evidence for a maximum in either of these samples at small periods. The intrinsic stress determined using substrate curvature is shown in figure 10(c)

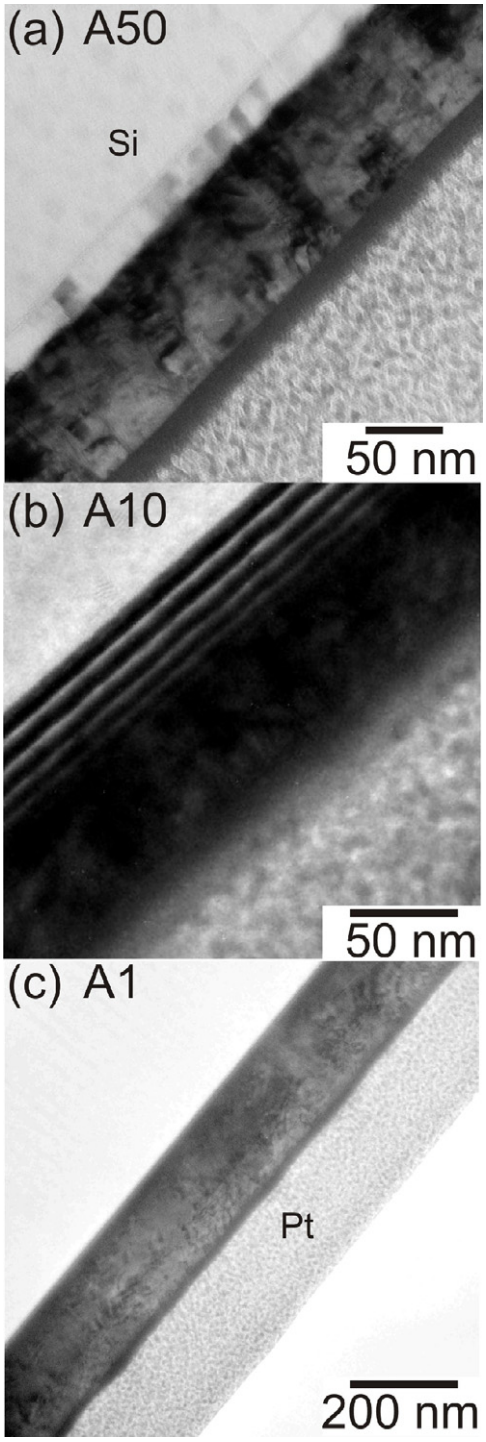

Figure 6. XTEM images of the 'A' series samples (a) A50, (b) A10 and (c) A1. Note that the Al layers are present during the initial stages of growth in (a) and (b).

for the 'A' series samples. There is a strong positive correlation between stress and both hardness and modulus.

4. Discussion

The sputtered films in the 'S' series are a good example of multilayer structures, with a constant thickness throughout

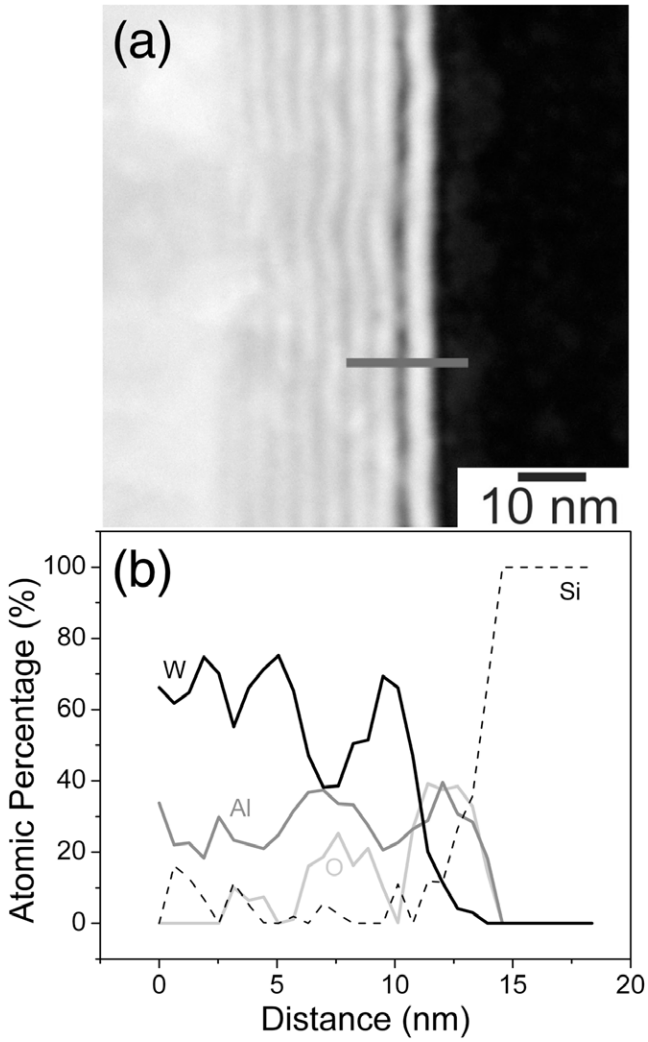

Figure 7. (a) High angle annular dark field STEM image of sample A10 along with (b) an EDS line scan through several layers as shown in (a). The EDS results show that O is present in the Al layers in decreasing concentration as deposition proceeds.

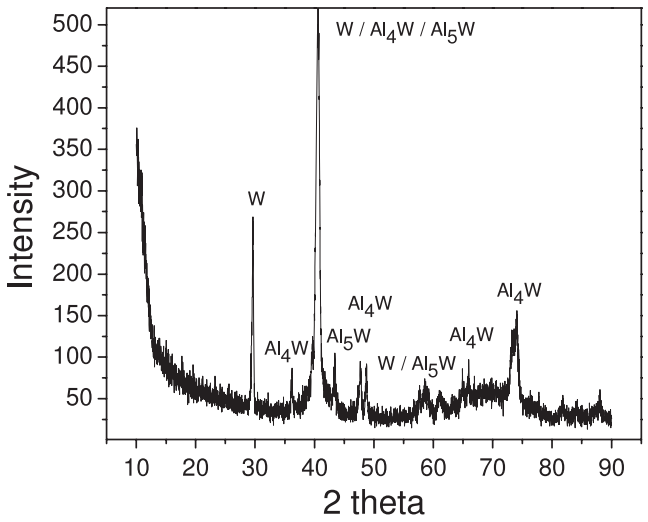

Figure 8. X-ray diffraction pattern for sample A1. The major lines have been indexed to W as well as Al_4W and Al_5W intermetallics [18].

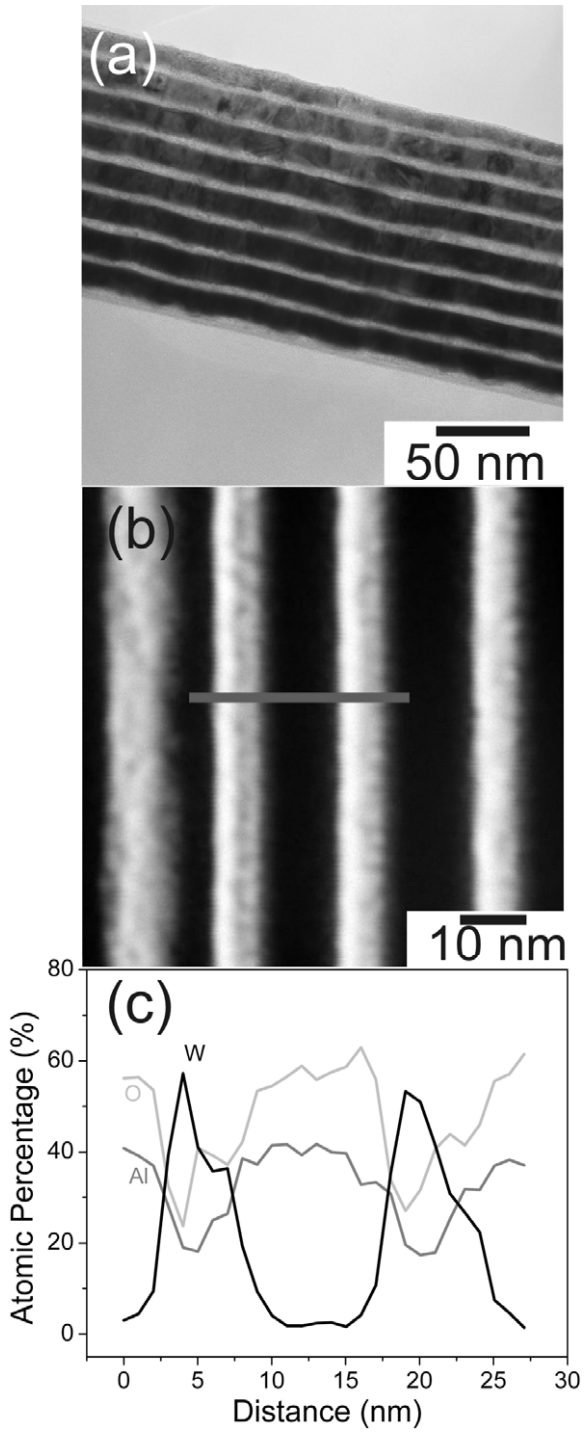

Figure 9. (a) XTEM image of the cathodic arc deposited sample prepared in the presence of Ar, sample Ar25, (b) the corresponding image for the sample O20 prepared in the presence of O_2 and (c) an EDS line scan through several layers of sample O20 as indicated in (b).

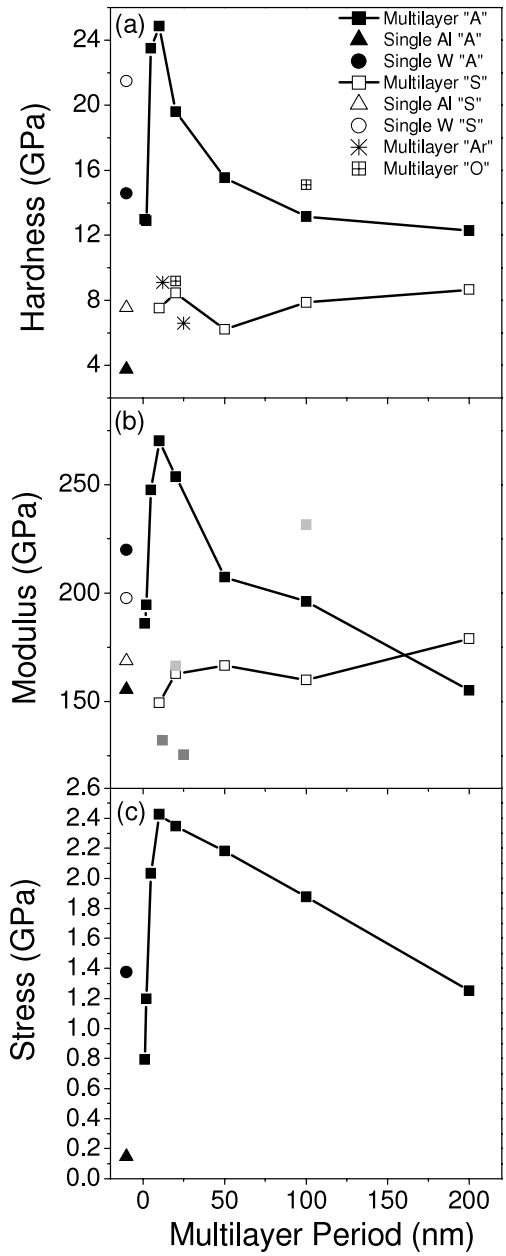

Figure 10. (a) The hardness and (b) the elastic modulus of all films plotted as a function their intended multilayer period. Also shown are results for single layers of W and Al 200 nm thick. (c) Shows the intrinsic stress as a function of intended multilayer period for the 'A' series samples only.

each constituent layer leading to a uniform periodic structure. Although O is present in the Al layers due to the gettering effect of Al during the sputter deposition process, these layers are mostly Al. The fact that there is no dependence of the hardness or the modulus on the period down to as small as 10 nm, rules out an enhancement effect due to the presence of multilayers in this system. Enhancement effects in multilayer structures are frequently reported [6, 7, 19, 20], however there are many reports which do not show such effects [21, 22]. A possible reason that the enhancement effect does not apply to the 'S' series is due to the very large layer roughness. This roughness reduces the effectiveness of the layers to act as a barrier for dislocation movement.

The films prepared using arc deposition in a vacuum ('A' series), are not true multilayer structures. In every case, Al was present in distinct layers only in the initial stages of the deposition. The majority of the coating consists of W, except when an intermetallic compound is formed due to energetic ion

induced mixing of the thin layers resulting in a process which is essentially co-deposition. The reason that an Al film does not nucleate on a W surface when the deposition is energetic as in the cathodic arc, as opposed to non-energetic in the case of sputtering, may have its origins in the mechanics of the film growth process. The Al ions in the cathodic arc have a most probable energy of approximately 50 eV [23]. SRIM [24] calculations show that backscatter of 50 eV Al ions incident on a W target is 35%. This, together with the weak bonding of Al to W and the effect of sputter etching, makes it difficult to form a layer of Al on a W surface. This explanation is supported by the observation that layers containing Al do nucleate and grow on W when another atomic species (Ar or O) is present. When a background gas is present, the incident energy of the Al ions will be reduced due to collisions in the gas phase, resulting in reduced backscatter and sputter etching. Gas phase collisions, as seen in previous work [25, 26], can result in a decrease of the ion energy and changes in the charge state distribution. This relationship is primarily a result of kinetic energy losses arising from collisions of ions with neutral background gas molecules. The presence of adsorbed gas molecules onto the W surface may also play an important role in promoting film growth. A collision between an incident Al ion and a stationary adsorbed gas atom or molecule is less likely to result in the backscattering of the Al because of the better match between masses. In the case of O being present on the W surface, the stronger chemical bonding between Al and O will further reduce the probability of Al being backscattered or sputter etched.

The thickness of the layer formed will depend on the balance between the incident flux and losses by backscattering and etching. The presence of O promotes deposition over backscattering/etching and as oxygen is depleted, the balance shifts. This was observed in the case of sample A10 (figure 6(b)) in which progressively thinner Al-containing layers are formed as O is depleted by gettering. Where excess O is maintained as in the 'O' series, periodic multilayer structures with constant layer thickness can be grown in the cathodic arc.

The arc samples prepared in a vacuum ('A' series) show a strong peak in hardness and modulus at an intended period of approximately 5–10 nm as shown in figure 10. Supporting evidence for the presence of a hardness maximum is provided by a maximum in intrinsic stress at the same nominal multilayer period. Intrinsic stress is generated in thin films deposited using energetic bombardment as a result of the effects of the ion impacts [27]. The stress will increase to a value limited by the yield strength of the film material. Therefore, the maximum in stress is expected to occur at the maximum in the hardness since both depend on the yield strength of the material.

The explanation for this peak does not lie in an effect that depends on the presence of multilayers, since the coatings showing enhanced hardness in figure 10 do not have a layered structure. In order to investigate this phenomenon further, samples A50 and A5 were examined using dark field microscopy. These images, shown in figure 11, have bright regions which identify the areas of the specimen that diffract strongly into an aperture receiving the tungsten {110} reflections. For example, the large bright region in sample A50 (figure 11(a)) identifies a strongly diffracting crystal of tungsten which extends throughout the structure even though an attempted deposition of Al was made periodically. However, the interruption caused by the attempt to deposit Al has an effect on the subsequent deposition. The region A corresponding to the initial W layer deposition is less defective than region B corresponding to the deposition after the attempted Al layer. As the frequency of attempted Al deposition increases, a greater defect density appears to be induced as shown in figure 11(b). The effective crystal size, indicated by the average size of the bright regions, becomes much smaller. We propose that the maximum in hardness in figure 10 is the result of an increase in defect density (caused by the attempted deposition of energetic Al ions) leading to a decrease in effective crystal size.

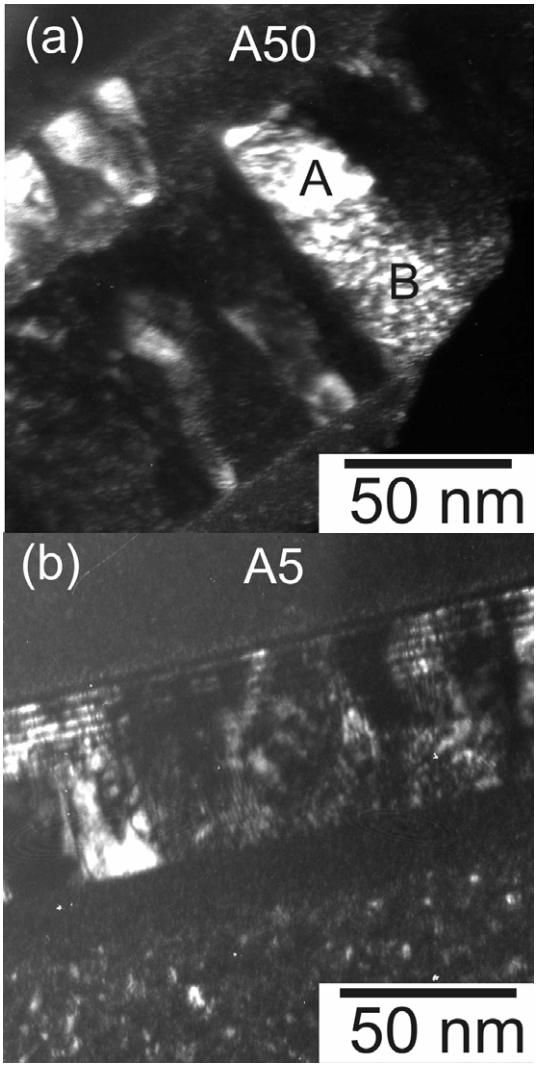

Figure 11. Dark field images taken using the tungsten {110} and aluminium {111} reflections of the pulsed cathodic arc deposited multilayer samples with a period of (a) 50 nm and (b) 5 nm.

The effect of the crystal size in a polycrystalline material on the yield stress, and therefore the hardness, has been

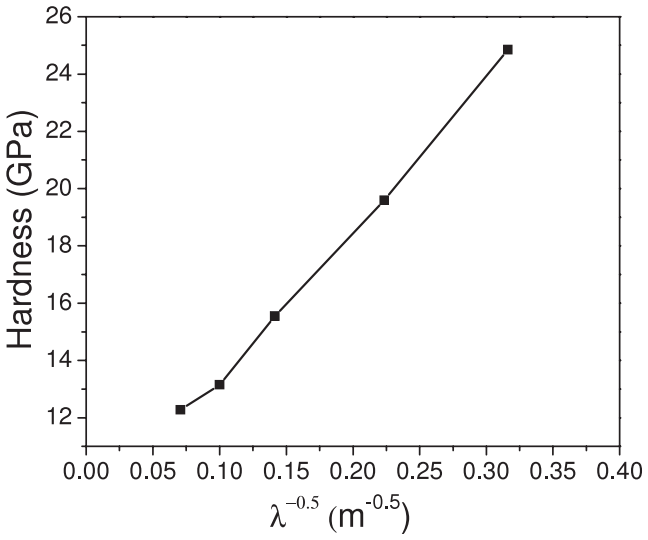

Figure 12. The measured indentation hardness plotted as a function of the square root of the inverse nominal period, as described by the Hall–Petch relation.

quantified in the Hall–Petch relation [3, 28]. This relates the yield stress (σ_y) of polycrystalline materials to their grain diameter (d) according to

$$\sigma_y = \sigma_0 + \frac{k}{d^{0.5}} \tag{1}$$

where σ_0 and k are constants. The Hall–Petch theory can be applied to the case of multilayers if the interfaces are assumed to behave as obstacles for dislocations so that pile-ups occur. A modified Hall–Petch equation for hardness enhancements in multilayer coatings can therefore be written as

$$H = H_0 + \frac{k}{\lambda^{0.5}} \tag{2}$$

where H is the hardness, H_0 and k are constants and λ is the multilayer period. This relation can be applied to a single W layer deposited with interruptions corresponding to attempted deposition of Al layers if it is assumed that the interruptions result in the introduction of defects and a corresponding reduction in the effective crystal size. Figure 11(b) provides evidence for this. Figure 12 shows the measured indentation hardness plotted as a function of the square root of the inverse nominal period, which is a measure of the effective crystal size. The linear relation shown in the figure confirms that the Hall–Petch relation holds for this set of samples.

5. Conclusions

Two techniques for depositing Al/W multilayers, namely sputtering and cathodic arc deposition produced very different outcomes in both microstructure and mechanical properties. The sputtering technique successfully produced regular multilayer structures with periods between 10 and 200 nm, however, no hardness enhancements were observed. Under vacuum conditions, cathodic arc deposition did not produce well defined multilayer structures due to the difficulty of growing Al layers on a W surface with energetic deposition. Adding Ar or O_2 during the growth process enabled multilayer structures to be synthesized by changing the growth conditions for Al at the W surface.

The only dependence of hardness on nominal period we observed was for the films deposited by cathodic arc under vacuum conditions which failed to produce consistent Al layers. A trend of increasing hardness and modulus was observed as the number of interruptions due to attempted Al layer deposition was increased. This behaviour was explained by a Hall–Petch model in which an increase in the density of defects in the W component of the structure was caused by the interruptions. These defects produce pinning sites for dislocations, resulting in an increase in hardness. The trend of enhanced hardness is halted at fine periods where intimate mixing of W and Al resulted in the formation of soft intermetallics.

The results presented in this paper show that defect density is the significant parameter that determines the hardness of a film and not the mere presence of multilayers. Without a complete understanding of the film microstructure, analysis of hardness enhancement effects is incomplete.

Acknowledgments

The authors gratefully acknowledge the assistance and comments by D J H Cockayne (Oxford University, UK), J Du Plessis (RMIT University, Melbourne), André Anders (Lawrence Berkeley National Laboratory, USA) and J E Bradby (Australian National University), in addition to JEOL Demonstration Laboratories in Akishima, Tokyo. Also acknowledged is the financial support granted by the Victorian Department of Innovation, Industry and Regional Development (DIIRD) and Australian Research Council (ARC).

References

[1] Anderson P M and Li C 1995 *Nanostruct. Mater.* **5** 349–62
[2] Friedman L H and Chrzan D C 1998 *Phys. Rev. Lett.* **81** 2715–8
[3] Hall E O 1951 *Proc. Phys. Soc.* B **64** 747–53
[4] Koehler J S 1970 *Phys. Rev.* B **2** 547–51
[5] Abadias G, Dub S and Shmegera R 2006 *Surf. Coat. Technol.* **200** 6538–43
[6] Helmersson U, Todorova S, Barnett S A, Sundgren J E, Markert L C and Greene J E 1987 *J. Appl. Phys.* **62** 481–4
[7] Madan A, Wang Y-y, Barnett S A, Engstrom C, Ljungcrantz H, Hultman L and Grimsditch M 1998 *J. Appl. Phys.* **84** 776–84
[8] Shinn M, Hultman L and Barnett S A 1992 *J. Mater. Res.* **7** 901–11
[9] Xiao X L, McCulloch D G, McKenzie D R and Bilek M M M 2006 *J. Appl. Phys.* **100** 1–8
[10] Fabreguette F H, Wind R A and George S M 2006 *Appl. Phys. Lett.* **88** 013116
[11] Anders A 1997 *Phys. Rev.* E **55** 969–81
[12] Oks E M, Anders A and Brown I G 1996 *IEEE Trans. Plasma Sci.* **24** 1174–83
[13] Mattox D M 1998 *Handbook of Physical Vapor Deposition (PVD) Processing* (Park Ridge: Noyes)

[14] Bilek M M M, Tarrant R N, McKenzie D R, Lim S H N and McCulloch D G 2002 *IEEE Trans. Plasma Sci.* **31** 939–44
[15] Brown I G 1998 *Annu. Rev. Mater. Sci.* **28** 243–69
[16] Oates T W H, Pigott J, McKenzie D R and Bilek M M M 2003 *Rev. Sci. Instrum.* **74** 4750–4
[17] Giannuzzi L A and Stevie F A 1999 *Micron* **30** 197–204
[18] Stubicar M, Tonejc A and Radic N 2001 *Vacuum* **61** 309–16
[19] Chu X, Wong M S, Sproul W D and Barnett S A 1993 *Surf. Coat. Technol.* **61** 251–6
[20] Tench D and White J 1984 *Metall. Trans.* A **15** 2039–40
[21] Lattemann M and Ulrich S 2007 *Surf. Coat. Technol.* **201** 5564–9
[22] Wong M-S, Hsiao G-Y and Yang S-Y 2000 *Surf. Coat. Technol.* **133/134** 160–5
[23] Anders A and Yushkov G Y 2002 *J. Appl. Phys.* **91** 4824–32
[24] Ziegler J F SRIM & TRIM: particle interaction with matter http://www.srim.org/
[25] Bilek M M M, Martin P J and McKenzie D R 1998 *J. Appl. Phys.* **83** 2965
[26] Rosen J, Anders A, Mraz S, Atiser A and Schneider J M 2006 *J. Appl. Phys.* **99** 1–5
[27] Davies K E, Gan B K, McKenzie D R, Bilek M M M, Taylor M B, McCulloch D G and Latella B A 2004 *J. Phys.: Condens. Matter* **16** 7947–54
[28] Petch N J 1953 *J. Iron Steel Inst.* **173** 25